

The last breath of the young gigahertz-peaked spectrum radio source PKS 1518+047

M. Orienti^{1,2*}, M. Murgia^{2,3}, D. Dallacasa^{4,2}

¹ *Instituto de Astrofísica de Canarias, c/ Vía Láctea s/n, E-38205 La Laguna (Tenerife), Spain*

² *INAF – Istituto di Radioastronomia, Via P. Gobetti 101, I-40129 Bologna, Italy*

³ *INAF – Osservatorio Astronomico di Cagliari, Poggio dei Pini, Strada 54, 09012 Capoterra (CA), Italy*

⁴ *Dipartimento di Astronomia, Università di Bologna, via Ranzani 1, I-40127, Bologna, Italy*

Received 13 February 2022; accepted ?

ABSTRACT

We present the results from multi-frequency VLBA observations from 327 MHz to 8.4 GHz of the gigahertz-peaked spectrum radio source PKS 1518+047 (4C 04.51) aimed at studying the spectral index distribution across the source. Further multi-frequency archival VLA data were analysed to constrain the spectral shape of the whole source. The pc-scale resolution provided by the VLBA data allows us to resolve the source structure in several sub-components. The analysis of their synchrotron spectra showed that the source components have steep spectral indices, suggesting that no supply/re-acceleration of fresh particles is currently taking place in any region of the source. By assuming the equipartition magnetic field of 4 mG, we found that only electrons with $\gamma \leq 600$, are still contributing to the radio spectrum, while electrons with higher energies have been almost completely depleted. The source radiative lifetime we derived is 2700 ± 600 years. Considering the best fit to the overall spectrum, we find that the time in which the nucleus has not been active represents almost 20% of the whole source lifetime, indicating that the source was 2150 ± 500 years old when the radio emission switched off.

Key words: radio continuum: general – galaxies: evolution – radiation mechanisms: non-thermal

1 INTRODUCTION

The radio emission of extragalactic powerful radio sources is due to synchrotron radiation from relativistic particles with a power-law energy distribution. They are produced in the “central engine”, namely the active galactic nucleus (AGN), and reaccelerated in the hot spot, that is the region where the particles, channelled through the jets, interact with the external medium. The energy distribution of the plasma is described by a power-law: $N(E) = N_0 E^{-\delta}$ that results in a power-law radio spectrum $S_\nu \propto \nu^{-\alpha}$, with a moderate steepening $S_\nu \propto \nu^{-\alpha+0.5}$ caused by energy losses in the form of radio emission. The spectral steepening occurs at the break frequency, ν_b , which is related to the age of relativistic electrons (see e.g. Pacholczyk 1970). This model, known as the *continuous injection* (CI) model, requires a continuous injection of power-law distributed electrons into a volume permeated by a constant magnetic field. The model has been applied to the interpretation of the total spectra of the radio sources (see e.g. Murgia et al.

1999), assuming that the emission of the lobes (supposed to have a constant and uniform magnetic field) dominates over that of core, jets and/or hot spots.

It is nowadays clear that powerful radio sources represent a small fraction of the population of the active galactic nuclei associated with elliptical galaxies, implying that the radio activity is a transient phase in the life of these systems. The onset of radio activity is currently thought to be related to merger or accretion events occurring in the host galaxy.

The evolutionary stage of each powerful radio source is indicated by its linear size. Intrinsically compact radio sources with linear size $LS \leq 1$ kpc, are therefore interpreted as young radio objects in which the radio emission originated a few thousand years ago (e.g. Fanti et al. 1995; Snellen et al. 2000). These sources are characterised by a rising synchrotron spectrum peaking at frequencies around a few gigahertz and are known as gigahertz-peaked spectrum (GPS) objects. When imaged with high resolution, they often display a two-sided morphology which looks like a scaled-down version of the classical and large (up to a few Mpc) double radio sources (Phillips & Mutel 1982). For these sources, kinematic (Polatidis & Conway 2003)

* E-mail: orienti@ira.inaf.it

and radiative (Murgia 2003) studies provided ages of the order of 10^3 and 10^4 years, supporting the idea that they are young radio sources whose fate is probably to become classical doubles. However, it has been claimed (Alexander 2000; Marecki et al. 2006) that a fraction of young radio sources would die in an early stage, never becoming the classical extended radio galaxies with linear sizes of a few hundred kpc and ages of the order of $10^7 - 10^8$ yr. Support for this scenario comes from a statistical study of GPS sources by Gugliucci et al. (2005): they showed that the age distribution of the small radio sources they considered has a peak around 500 years.

So far, only a few objects have been recognised as dying radio sources. They are difficult to find owing to their extremely steep radio spectrum which makes them under-represented in flux-limited catalogues. The objects 0809+404 (Kunert-Bajraszewska et al. 2006) and 1542+323 (Kunert-Bajraszewska et al. 2005) are possible examples of young radio sources that are fading. These sources, with an estimated age of $10^4 - 10^5$ years, have been suggested as “faders” due to the lack of active structures, like cores and hot-spots, although their optically-thin radio spectra do not display the typical form expected for a fader.

In this paper, we present results from multi-frequency VLBA and VLA data of the GPS radio source PKS 1518+047 (RA=15^h 21^m 14^s and DEC=04° 30′ 21″, J2000), identified with a quasar at redshift $z = 1.296$ (Stickel & Kuhr 1996). It is a powerful radio source ($\text{Log } P_{1.4\text{GHz}} (\text{W/Hz}) = 28.53$), with a linear size of 1.28 kpc. This source was selected from the GPS sample of Stanghellini et al. (1998) on the basis of its steep spectrum $\alpha_{1.4\text{GHz}}^{8.4\text{GHz}} = 1.2$, uncommon in young radio sources. The goal of this paper is to determine by means of the analysis of the radio spectrum and its slope in the optically thin region, whether this source is in a phase where its radio activity has, perhaps temporarily, switched off.

Throughout this paper, we assume the following cosmology: $H_0 = 71 \text{ km s}^{-1} \text{ Mpc}^{-1}$, $\Omega_M = 0.27$ and $\Omega_\Lambda = 0.73$, in a flat Universe. At the redshift of the target $1'' = 8.436 \text{ kpc}$. The spectral index is defined as $S(\nu) \propto \nu^{-\alpha}$.

2 RADIO DATA

The target source was observed on March 5, 2008 (project code BD129) with the VLBA at 0.327, 0.611 (P band), 1.4 and 1.6 GHz (L band) with a recording band width of 16 MHz at 256 Mbps for 20 min in L band and 1 hr in P band. The correlation was performed at the VLBA correlator in Socorro. These observations have been complemented with archival VLBA data at 4.98 (C band) and 8.4 GHz (X band) carried out on March 28, 2001 (project code BS085). The data reduction was carried out with the NRAO AIPS package.

During the observations, the gain corrections were found to have variations within 5% in L, C and X bands, and 10% in P band respectively. In P band, the antennas located in Kitt Peak, Mauna Kea and North Liberty had erratic system temperatures, probably due to local RFI, and their

Freq. GHz	Tot ^a mJy	N ^b mJy	S ^b mJy
0.32	2278±38	1136±117	512±58
0.61	4050±200 ^c	1778±182	897±98
0.96	4720±240 ^d	-	-
1.4	3937±120	2468±123	1555±78
1.6	3376±101	2008±101	1311±56
3.9	1460±50 ^d	-	-
4.5	1164±30	-	-
4.9	1013±30	392±19	479±24
5.0	994±52 ^e	-	-
8.1	486±15	-	-
8.4	441±13	148±7	232±11
11.1	305±30 ^d	-	-
15	165±1	-	-
22	80±5	-	-

Table 1. Multi-frequency flux density of PKS 1518+047 and of its northern and southern components. *a* = archival VLA data; *b* = VLBA data; *c* = WSRT data from Stanghellini et al. (1998); *d* = RATAN data from Stanghellini et al. (1998); *e* = WSRT data from Xiang et al. (2006).

data had to be flagged out completely. The resulting loss of both resolution and sensitivity did not affect the source structure and flux density.

To constrain the spectral shape of the whole source, we analysed archival VLA data at 0.317, 1.365, 1.665, 4.535, 4.985, 8.085, 8.465, 14.940 and 22.460 GHz, obtained on August 22, 1998 (project code AS637). The data reduction was carried out with the standard procedure implemented in the NRAO AIPS package. Uncertainties in the determination of the flux density are dominated by amplitude calibration errors, which are found to be around 3% at all frequencies.

VLA and VLBA final images were obtained after a number of phase-only self-calibration iterations. At 4.9 and 8.4 GHz, besides the *full resolution* VLBA image, we also produced a *lower resolution* image using the same *uv*-range, image sampling and restoring beam of the 1.6 GHz, in order to produce spectral index maps of the source. Images at the various frequencies were aligned using the task LGEOM by comparing the position of the compact and bright components at each frequency.

Flux density and deconvolved angular sizes were measured by means of the task JMFIT which performs a Gaussian fit to the source components on the image plane, or, in the case of extended components, by TVSTAT which performs an aperture integration on a selected region on the image plane.

The parameters derived in this way are reported in Table 1. About 8% and 20% of the total flux density is missing in our VLBA images at 4.9 and 8.4 GHz respectively if we consider the VLA measurements. It is likely that such a missing flux density is from a steep-spectrum and diffuse emission which is not sampled by the VLBA data due to the lack of appropriate short spacings.

3 RESULTS

3.1 Source structure

Multi-frequency VLBA observations with parsec-scale resolution allow us to resolve the structure of PKS 1518+047 into two main source components (Fig. 1), separated by 135 mas (1.1 kpc), in agreement with previous images by Dallacasa et al. (1998), Xiang et al. (2002), and Xiang et al. (2006). Both the northern and southern components have angular size of $23 \times 15 \text{ mas}^2$.

At the highest frequencies, where we achieve the best resolution, the northern component is resolved into two sub-structures (labelled N1 and N2) separated by 11 mas (90 pc) and position angle of 11° . N1 accounts for 295 and 119 mJy at 4.9 and 8.4 GHz, respectively, with angular size of $7.7 \times 6.8 \text{ mas}^2$. Component N2 is fainter than N1 and it accounts for 97 and 29 mJy at 4.9 and 8.4 GHz, respectively, with angular size of $7.4 \times 5 \text{ mas}^2$. The southern complex is resolved into 4 compact regions located at 3, 7 and 16 mas (25, 60 and 130 pc for S2, S3 and S4 respectively) with respect to S1, all with almost the same position angle of 40° . The resolution, not adequate to properly fit the several components of the southern lobe, does not allow us to reliably determine the observational parameters of each single sub-component.

The spectral index in both the northern and southern complexes, computed considering the integrated component flux density, is steep, with $\alpha_{1.4}^{8.4} = 1.5 \pm 0.1$ and $= 1.0 \pm 0.1$, respectively. Errors on the spectral indices were calculated following the error propagation theory. The analysis of the spectral index distribution in the southern complex (Fig. 2) shows a steepening of the spectral index going from S1 inwards to S4, suggesting that S1 is likely the last place where relativistic electrons coming from the source core were re-accelerated. In the northern lobe, the spectral index between 1.6 and 4.9 GHz is almost constant across the component, showing a small gradient going from N1 towards N2, while in the spectral index maps at higher frequencies it steepens from N1 to N2 (Fig. 2). The steep spectral indices showed by the northern and southern components suggest that no current particle acceleration across the source is taking place, indicating that active regions, like conventional jet-knots and hot spots, are no longer present.

At 327 and 611 MHz, i.e. in the optically-thick part of the spectra, the low spatial resolution does not allow us to separate the individual sub-components. However, their spectral indices, obtained considering the integrated flux density, are $\alpha_{327}^{611} \sim -0.6 \pm 0.2$ and -0.9 ± 0.2 for the northern and southern component respectively, that is much flatter than the value expected in the presence of “classical” synchrotron self-absorption from a homogeneous component, indicating that what we see is the superposition of the spectra of the various sub-components, each characterised by its own spectral peak occurring in a range of frequencies and then causing the broadening of the overall spectrum (i.e. the northern and southern components are far from being homogeneously filled by magnetised relativistic plasma).

3.2 The spectral shape

To understand the physical processes taking place in this source we fit the optically-thin part of the overall spectrum, as well as the spectra of the northern and southern components, assuming two different models. The first model assumes that fresh relativistic particles are continuously injected in the source (*CI model*), while in the second model the continuous supply of particles is over and the radio source is already in the relic phase (*CI OFF model*).

The CI synchrotron model is described by three parameters:

- i) α_{inj} , the injection spectral index;
- ii) ν_b , the break frequency;
- iii) $norm$, the flux normalization.

As the injection of fresh particles stops (CI OFF model), a second break, ν_{b2} , appears at high frequencies, and beyond that the spectrum cuts off exponentially. This second break is related to the first according to:

$$\nu_{b2} = \nu_b \left(\frac{t_s}{t_{OFF}} \right)^2 \quad (1)$$

where t_s is the total source’s age and t_{OFF} is the time elapsed since the injection switched off (see e.g. Komissarov & Gubanov 1994; Slee et al. 2001; Parma et al. 2007). Indeed, compared to the basic CI model, the CI OFF model is characterized by one more free parameter:

- i) α_{inj} , the injection spectral index;
- ii) ν_b , the lowest break frequency;
- iii) $norm$, the flux normalization;
- iv) t_{OFF}/t_s , i.e. the relic to total source age ratio.

The spectral shapes of both models cannot be described by analytic equations and must be computed numerically (see e.g. Murgia et al. 1999 and Slee et al. 2001 for further details).

In the study of the overall spectrum, in addition to the archival VLA data analysed in this paper, we consider also RATAN observations at 0.96, 3.9, and 11.1 GHz (Stanghellini et al. 1998), and WSRT observations at 5 GHz (Xiang et al. 2006), to have a better frequency sampling. Due to the presence of another radio source located at about 1 arcminute from the target (Fig. 3), we do not consider observations with resolution worse than $\sim 1'$.

During the fitting procedure, a particular care was taken in choosing the most accurate injection spectral index. The peculiar shape of the radio spectrum of this source does not allow us to directly derive the injection spectral index from the optically-thin emission below the break, because it falls below the peak frequency where the spectrum is absorbed. For this reason, we fit the spectrum assuming various injection spectral indices, choosing the one that provides the best reduced chi-square (Fig. 4c).

The best fit we obtain with the CI model implies a very steep injection spectral index $\alpha_{inj} = 1.1$, that is reflected in an uncommon electron energy distribution $\delta = 3.2$, (Fig. 4a). On the other hand, the CI OFF model provides a more common injection spectral index $\alpha_{inj} = 0.7$ (Fig. 4b). Furthermore, the comparison between the reduced chi-square of

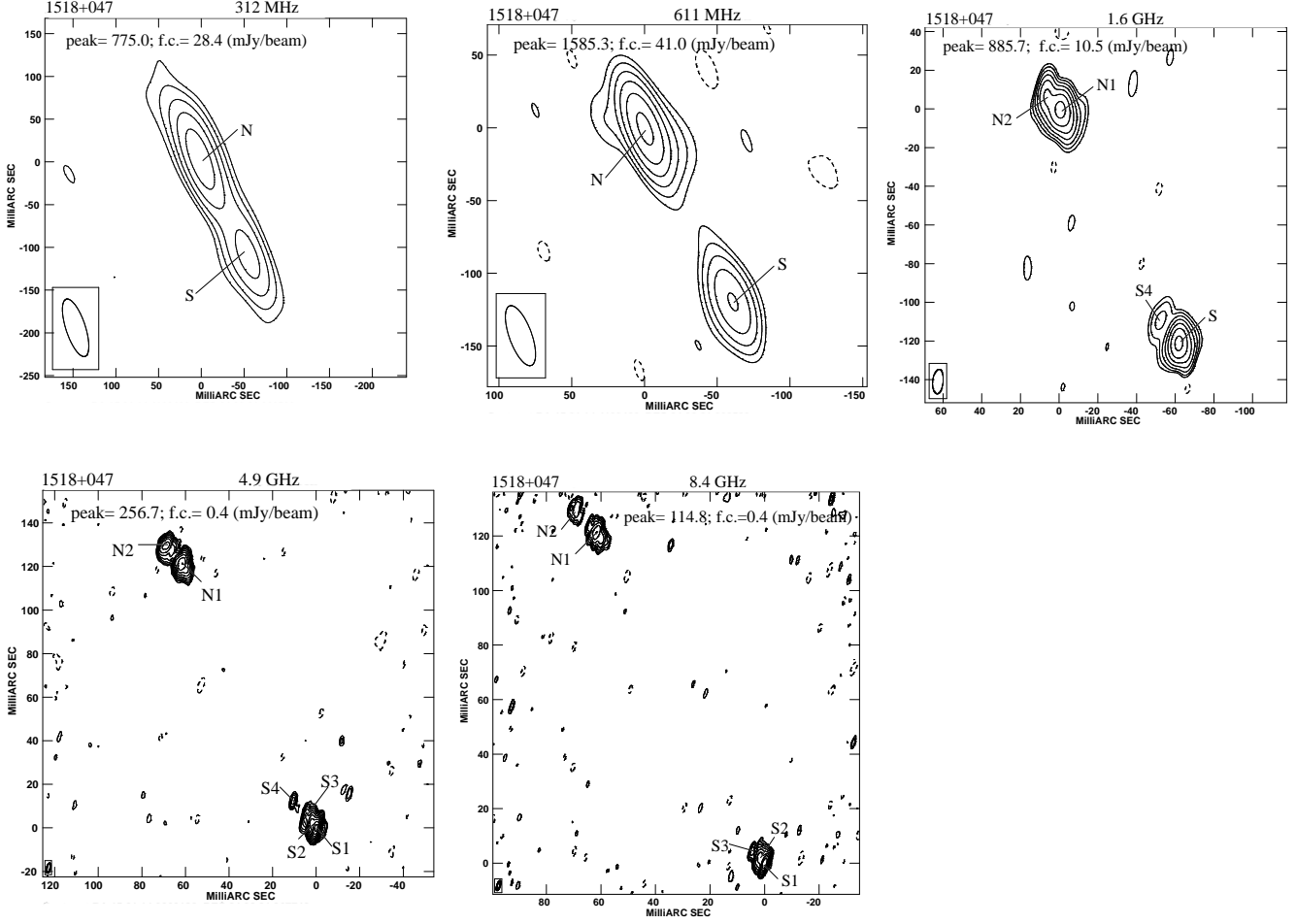


Figure 1. VLBA images at 0.327, 0.611, 1.6, 4.9 and 8.4 GHz of PKS 1518+047. On the images we show the observing frequency, the peak flux density and the first contour intensity (f.c.) which is 3 times the 1σ noise level measured on the image plane. Contours increase of a factor 2. The beam is plotted on the bottom left corner.

the different models (Fig. 4c) shows that the CI OFF model is more accurate in fitting the data. In the context of the CI OFF model, we derive a break frequency $\nu_{\text{br}} = 2.4$ GHz, and $t_{\text{OFF}}/t_s = 0.2$. A similar result is found for the spectrum of the southern component. As in the overall spectrum, both CI and CI OFF models well reproduce the spectral shape (Fig. 5), but the former implies an uncommonly steep injection spectral index.

A different result is found in the analysis of the northern lobe. In this case, we find that the CI OFF model with $\alpha_{\text{inj}} = 0.7$ well reproduces the spectral shape, providing a break frequency $\nu_{\text{br}} = 0.8$ GHz and $t_{\text{OFF}}/t_s \sim 0.27$ (Fig. 6b), while the CI model provides a worse chi-square even considering a steep injection spectral index (Fig. 6a).

The optically-thick part of the spectra is well modelled by an absorbed spectrum with $\alpha_{\text{thick}} = -1.2 \pm 0.1$, that is different from the canonical -2.5 expected in the presence of synchrotron self-absorption from a homogeneous component. This result, together with the source structure resolved in several sub-components, indicates that in the optically-thick regime the observed spectra are the superposition of the spectra of many components that cannot be

resolved due to resolution limitation.

The best fit parameters obtained with the CI and CI OFF models, and assuming synchrotron self-absorption (SSA) are reported in Table 2.

3.3 Physical parameters

Physical parameters for the radio source components were computed assuming equipartition condition and using standard formulae (Pacholczyk 1970). We considered particles with energy between $\gamma_{\text{min}} = 100$ and $\gamma_{\text{max}} = 600$. The high energy cut-off corresponds to the value for which the break frequency in the observer frame occurs at 2.4 GHz, as obtained from the best fit to the model (Section 3.2). Proton and electron energy densities are assumed to be equal, and the spectral index is $\alpha = 0.7$ (see Section 3.2). We assume that the volume V of the emitting regions is a prolate spheroid:

$$V = \frac{\pi}{6} ab^2 \phi$$

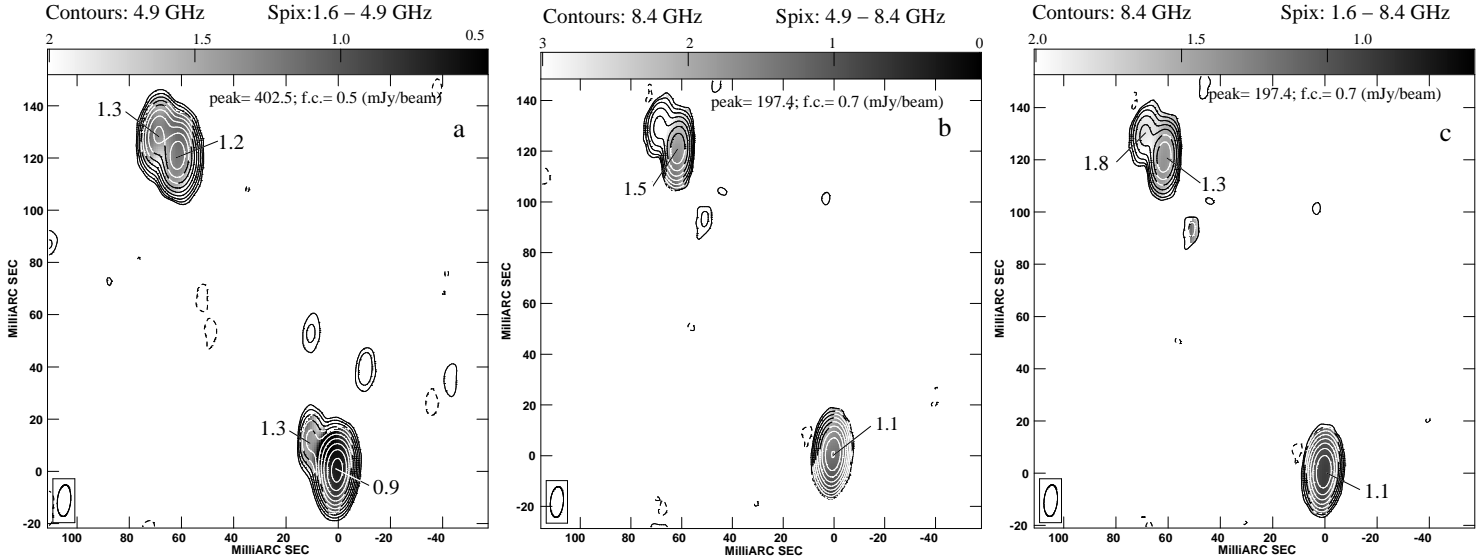


Figure 2. VLBA spectral index images of PKS 1518+047 between 1.6 and 4.9 GHz (*panel a*), between 4.9 and 8.4 GHz (*panel b*), and between 1.6 and 8.4 GHz (*panel c*). On the images we show the observing frequency of the contours, the peak flux density and the first contour intensity (f.c.) which is 3 times the 1σ noise level measured on the image plane. Contours increase of a factor 2. The beam is plotted on the bottom left corner. The grey scale is shown by the wedge at the top of each image.

where a and b are the spheroid major and minor axes, and ϕ is the filling factor. In the case of the entire radio source, we consider $a = 140$ mas, $b = 25$ mas, and $\phi = 1$. With these assumptions, we obtain an equipartition magnetic field $H_{\text{eq}} = 4$ mG, and a minimum energy density $u_{\text{min}} = 1.4 \times 10^{-6}$ erg/cm³. In the case of component N and S we assume $a = 23$ mas, $b = 15$ mas and $\phi = 1$, and we infer a magnetic field of 7 mG, and a minimum energy density of 5×10^{-6} erg/cm³, in agreement with the values derived for the entire source structure.

4 DISCUSSION

In general the shape of the synchrotron spectrum of active radio sources is the result of the interplay between freshly injected relativistic particles and energy losses that cause a depletion of high-energy particles which results into a steepening of the spectrum at high frequencies. The discovery of a GPS radio source, considered to be a young object where the radio emission started a few thousand years ago, but displaying a steep spectral index ($\alpha_{1.6}^{8.4} > 1.0$) in all its components is somewhat surprising. Indeed, the strong steepening found across the components of PKS 1518+047 is incompatible with the moderate high-frequency steepening predicted by a continuous injection of particles, suggesting that no injection/acceleration of fresh relativistic particles is currently occurring in any region of the source. Furthermore, when the injection of fresh particles is over, the strong adiabatic losses cause a fast shift of the spectral turnover towards lower frequencies and a decrement of the peak flux density. Therefore, detections of dying radio sources with a spectral peak still occurring in the GHz regime are extremely rare. A possible

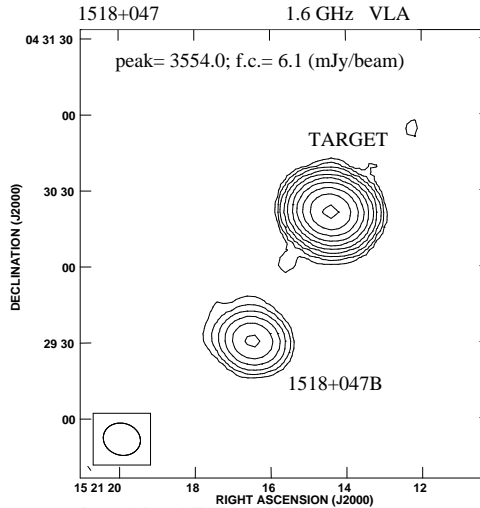


Figure 3. VLA image at 1.6 GHz of PKS 1518+047. Another source, 1518+047B, is located at ~ 1 arcminute in the south-east direction from the target.

explanation may arise from the presence of a dense ambient medium enshrouding the radio source which may confine the relativistic particles reducing the adiabatic losses. This is probably the case of fading radio sources found in galaxy clusters where the intracluster medium (ICM) is likely limiting adiabatic cooling (Slee et al. 2001). However, in the case of PKS 1518+047 the source is surrounded by the interstellar medium (ISM) of the host galaxy, but its confinement cannot be related to neutral hydrogen, because observations searching for H_I absorption did not provide evidence of a

Comp.	Model	α_{inj}	ν_{p} MHz	ν_{b} MHz	t_{OFF}/t_s	χ_{red}^2
N	CI	1.1	1300^{+80}_{-80}	870^{+630}_{-440}	-	12.0
N	CI OFF	0.7	1620^{+380}_{-280}	800^{+1230}_{-410}	0.27	5.4
S	CI	1.1	1400^{+880}_{-190}	<35000	-	0.7
S	CI OFF	0.7	1720^{+880}_{-540}	1260^{+15870}_{-1110}	>0.01	0.57
Tot	CI	1.1	1050^{+46}_{-40}	7130^{+1740}_{-1470}	-	5.6
Tot	CI OFF	0.7	1000^{+110}_{-74}	2380^{+1130}_{-950}	0.21	0.46

Table 2. Best fit parameters obtained with the CI and CI OFF models + SSA for the source PKS 1518+047 and for its northern and southern components.

dense environment (Gupta et al. 2006).

From the analysis of the optically-thin spectrum of PKS 1518+047, we find that the steepening may be explained assuming that the supply of relativistic plasma is still taking place, but the energy distribution of the injected particles is uncommonly steep. Another explanation is that the steep spectral shape is due to the absence of freshly injected/reaccelerated particles and the energy losses are driving the spectrum evolution. Support to this scenario comes from the best fit to the spectrum of the northern component, where the continuous injection model fails in reproducing the spectral shape, even assuming that relativistic particles are injected with a steep energy distribution. This steep spectrum can be best reproduced by a synchrotron model in which no particle supply is taking place. Furthermore, the time spent by the source in its “fader” phase is about 20% of the whole source age.

We estimate the break energy γ_{b} of the electron spectrum and the electron radiative time by:

$$\gamma_{\text{b}} \sim 487 \nu_{\text{b}}^{1/2} H^{-1/2} (1+z)^{1/2} \quad (2)$$

and

$$t_s = 5.03 \times 10^4 H^{-3/2} \nu_{\text{b}}^{-1/2} (1+z)^{-1/2} \quad (\text{yr}) \quad (3)$$

where H is in mG and ν_{b} in GHz.

If in Eqs. 2 and 3 we consider the equipartition magnetic field and ν_{b} derived from the fits, we find that the energy of the electrons responsible for the break should be $\gamma \sim 400 - 600$ and the source radiative lifetime is $t_s = 2700 \pm 600$ yr. As a consequence, electrons with $\gamma > 600$ (i.e. with shorter radiative lifetime) have already depleted their energy and they contribute only to the high-frequency tail of the spectrum.

If we consider the $t_{\text{OFF}}/t_s \sim 0.2$, as derived from the fit to the overall spectrum, we find that $t_{\text{OFF}} = 550 \pm 100$ years, and this represents the time elapsed since the last supply/acceleration of relativistic particles. These values indicate that the radio source was 2150 ± 500 years old when the radio emission switched off.

The small t_{OFF} derived suggests that adiabatic losses had not enough time to shift the spectral peak of PKS 1518+047 far from the GHz regime. In the presence of adiabatic expansion, and considering a magnetic field frozen in the plasma, the spectral peak is shifted towards lower frequencies:

$$\nu_{p,1} = \nu_{p,0} \left(\frac{t_0}{t_1} \right)^4 \quad (4)$$

where $\nu_{p,0}$ and $\nu_{p,1}$ are the peak frequency at the time t_0 and t_1 respectively (Orienti & Dallacasa 2008). As the time elapsed after the switch off increases, the peak moves to lower and lower frequencies, making the source unrecognisable as a young GPS. For example, when t_{OFF} will represent more than 40% of the total source lifetime, the peak should be below 300 MHz, so it will be difficult to identify as a dying young radio source. Future instruments like LOFAR may unveil a population of such fading radio sources.

5 CONCLUSIONS

We presented results from multi-frequency VLBA and VLA observations of the GPS radio source PKS 1518+047. The analysis of the spectral index distribution across the whole source structure showed that all the source components have very steep optically-thin synchrotron spectra. The radio spectra are well explained by energy losses of relativistic particles after the cessation of the injection of new plasma in the radio lobes. This result, together with the lack of the source core and active non-steep spectrum components like hot spots and knots in the jets, suggests that no injection/acceleration of fresh particle is currently occurring in any region of the source. For this reason, PKS 1518+047 can be considered a fading young radio source, in which the radio emission switched off shortly after its onset. When the supply of energy is switched off, given the high magnetic fields in the plasma, the spectral turnover moves rapidly towards low frequencies, making the source undetectable at the frequencies commonly used for radio surveys. However, in PKS 1518+047 the time elapsed since the last particle acceleration is of the order of a few hundred years, suggesting that PKS 1518+047 still has a GPS spectrum because adiabatic losses have not had enough time to affect the source spectrum, shifting the peak far from the GHz regime. If the interruption of the radio activity is a temporary phase and the radio emission from the central engine will re-start soon, it is possible that the source will appear again as a GPS without the severe steepening at high frequencies. If this does not happen, the fate of this radio source is to emit at lower and lower frequencies,

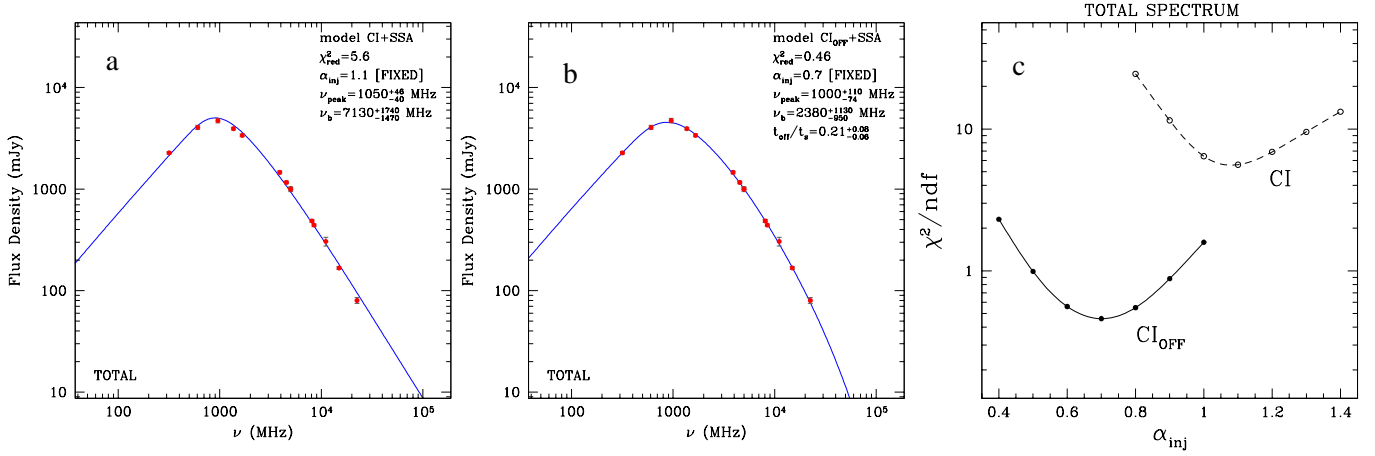


Figure 4. The best fit to the overall spectrum of PKS 1518+047 using the CI (*left*) and the CI OFF models (*center*), and the reduced chi-square versus the injection spectral index (*right*). Error bars are rather small, and often result within the symbol.

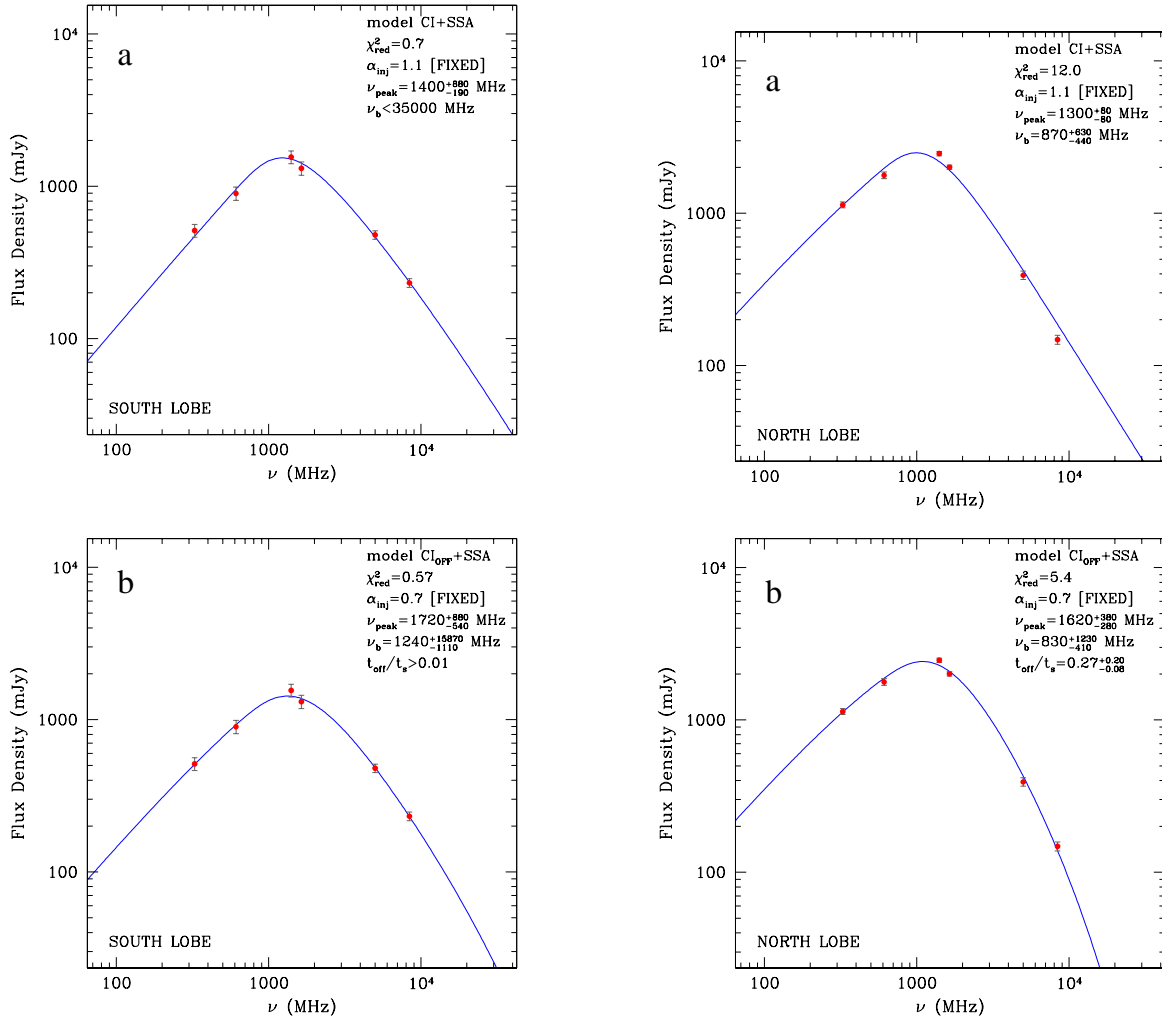


Figure 5. The best fit to the spectrum of the southern component of PKS 1518+047 using the CI (*top*) and the CI OFF models (*bottom*).

Figure 6. The best fit to the spectrum of the northern component of PKS 1518+047 using the CI (*top*) and the CI OFF models (*bottom*).

until it disappears at frequencies well below the MHz regime.

ACKNOWLEDGEMNET

We thank the anonymous referee for carefully reading the manuscript and valuable suggestions. The VLBA is operated by the US National Radio Astronomy Observatory which is a facility of the National Science Foundation operated under a cooperative agreement by Associated University, Inc. This work has made use of the NASA/IPAC Extragalactic Database (NED), which is operated by the Jet Propulsion Laboratory, California Institute of Technology, under contract with the National Aeronautics and Space Administration.

REFERENCES

- Alexander, A., 2000, MNRAS, 319, 8
Dallacasa, D., Bondi, M., Alef, W., Mantovani, F., 1998, A&AS, 129, 219
Fanti, C., Fanti, R., Dallacasa, D., Schilizzi, R. T., Spencer, R. E., Stanghellini, C., 1995, A&A, 302, 317
Gugliucci, N.E., Taylor, G.B., Peck, A.B., Giroletti, M., 2005, ApJ, 622, 136
Gupta, N., Salter, C.J., Saikia, D.J., Ghosh, T., Jeyakumar, S., 2006, MNRAS, 373, 972
Komissarov, S.S., Gubanov, A.G., 1994, A&A, 285, 27
Kunert-Bajraszewska, M., Marecki, A., Thomasson, P., Spencer, R. E., 2005, A&A, 440, 93
Kunert-Bajraszewska, M., Marecki, A., Thomasson, P., 2006, A&A, 450, 945
Marecki, A., Kunert-Bajraszewska, M., Spencer, R.E., 2006, A&A, 449, 985
Murgia, M., Fanti, C., Fanti, R., Gregorini, L., Klein, U., Mack, K.-H., Vigotti, M., 1999, A&A, 345, 769
Murgia, M., 2003, PASA, 20, 19
Orienti, M., Dallacasa, D., 2008, A&A, 477, 807
Pacholczyk, A.G., 1970, Radio Astrophysics, (San Francisco: Freeman & Co.)
Parma, P., Murgia, M., de Ruiter, H.R., Fanti, R., Mack, K.-H., Govoni, F., 2007, A&A, 470, 875
Phillips, R.B., Mutel, R.L., 1982, A&A, 106, 21
Polatidis, A.G., & Conway, J.E., 2003, PASA, 20, 69
Slee, O.B., Roy, A.L., Murgia, M., Andernach, H., Ehle, M., 2001, AJ, 122, 1172
Snellen, I. A. G., Schilizzi, R. T., Miley, G. K., de Bruyn, A. G., Bremer, M. N., Röttgering, H. J. A., 2000, MNRAS, 319, 445
Stanghellini, C., O’Dea, C.P., Dallacasa, D., Baum, S.A., Fanti, R., Fanti, C., 1998, A&AS, 131, 303
Stickel, M., Kuhr, H., 1996, A&AS, 115, 11
Xiang, L., Stanghellini, C., Dallacasa, D., Haiyan, Z., 2002, A&A, 385, 768
Xiang, L., Reynolds, C., Strom, R.G., Dallacasa, D., 2006, A&A, 454, 729